3-Dimensional Simulation of Plasma Dynamics in SPT[*†]

Vladimir Kim, Alexander Bishaev, Alexei Lazourenko
Research Institute of Applied Mechanics and Electrodynamics
of Moscow Aviation Institute (RIAME MAI),
5 Leningradskoe schosse, p/b 43, Moscow, 125080, Russia,
tel.: + 7 095 1580020, fax: + 7 095 1580367, riame@sokol.ru

Monika Auweter-Kurtz,
Institut für Raumfahrtsysteme (IRS),
Stuttgart University,
Pffafenwaldring 31, 70569 Stuttgart, Germany,
tel.: + 49 0711 685-2376, fax: + 49 0711 685-3596, auweter@irs.uni-stuttgart.de

IEPC-01-340

A kinetic approach is applied to model plasma dynamics in SPT accelerating channel. Magnetic field is assumed to be external, predefined and stationary. Atom and ion dynamics is simulated and experimental data on electron dynamics and near-wall electric potential distribution is utilized. Completely 3-D simulation was carried out for SPT-100 with thrust vector control unit (TVCU), having essentially azimuth nonsymmetrical magnetic field. Results of the simulation are in satisfactory agreement with the measurements of thrust and thrust vector deviation angle. Distributions of plasma macroparameters are in a well agreement with available data on local plasma measurements in SPT accelerating channel.

Introduction

Proper simulation of plasma behavior in the accelerating channel of Hall thrusters is a difficult task due to the complexity of the processes are to be taken into account. Plasma flow in Hall thrusters has been simulated by Komurasaki and Arakawa [1], they employed a steady state, two-dimensional kinetic formulation. One-dimensional unsteady formulation was employed by Boeuf and Garrigues [2]. A hybrid, Monte-Carlo Collision-Particle in Cell approach was utilized by Boyd et al [3].

Authors of this work have developed an approach based on the model kinetic equations. Full statement of the problem on plasma dynamics in the SPT accelerating channel was presented in a paper [4]. Kinetic description of three plasma species - electrons, singly charged ions and neutrals - was utilized. In order to verify numerical algorithms and basic concepts that model was reduced to simpler one. Two following simplifications were introduced. First, electron dynamics is described on the base of experimental data. Second, near-wall sheaths do not considered. In the next section we review briefly main equations and necessary assumptions.

1.Statement of the Problem

1.1 Main equations

SPT accelerating channel scheme is presented in Fig1.

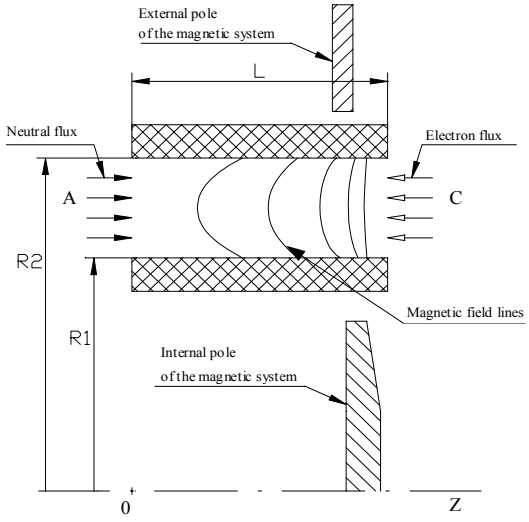

Fig. 1 Accelerating channel scheme.
A – anode side, C – cathode side.

[*] Presented as Paper IEPC-01-340 at the 27th International Electric Propulsion Conference, Pasadena, CA, 15-19 October, 2001.
[†] Copyright © by Vladimir Kim. Published by Electric Propulsion Society with Permission.

Plasma behavior in the SPT accelerating channel is described at the kinetic level [4]. The following components of plasma are considered: electrons, singly charged ions and neutrals. For ions and neutrals distribution functions $f^s(t,x,\xi)$ are introduced, where t – time, $x=\{x_i\}$, i=1,2,3 – coordinates in physical space, $\xi=\{\xi_i\}$ - coordinates in velocity space, s=1,2,3 – kind of particle (electrons, ions and neutrals, respectively; electrons are mentioned for the generality). Only stationary case is considered, i.e. $\frac{\partial}{\partial t}=0$. Macroparameters are defined by the following way:

$$\begin{pmatrix} n \\ nu \\ \frac{3}{2}nkT+\frac{\rho u^2}{2} \end{pmatrix}^s = \int \begin{pmatrix} 1 \\ \xi \\ \frac{m\xi^2}{2} \end{pmatrix}^s f^s d\xi, d\xi = d\xi_1 d\xi_2 d\xi_3 \quad (1)$$

where n – particle density, nu - particle flux density, T – temperature of the corresponding type of the particle. Thrust is calculated according to the formula:

$$F = m_2 \int_S \left(\int \xi^{(2)} \xi_z^{(2)} f^2 d\xi^{(2)} \right) dS, \quad (1a)$$

where integration in the external integral is performed over the area of the exit cross-section of the accelerating channel. The system of kinetic equations describing plasma motion in the accelerating channel can be represented in the general form as follows:

$$\left(\frac{Df^s}{Dt}\right)_{\xi^s} + \frac{e_s}{m_s} E_i \frac{\partial f^s}{\partial \xi_i^s} + \delta_{1s} \frac{e_s}{m_s c} \varepsilon_{ijk} H_k \xi_j^s \frac{\partial f^s}{\partial \xi_j^s} = I^s \quad (2)$$

where s=2,3; i=1,2,3; j=1,2,3; k=1,2,3. In (2) the following designations are accepeted: E_i – electric field components, e_s – charge of the particle (e_1=-e, e_2=e, e_3=0, e – electron charge module), H_k – magnetic field components. It is assumed that magnteic field does not affect ions and neutrals, therefore δ_{12}=0, δ_{13}=0, $\varepsilon_{i,j,k}$ Levi-Chevita tensor. $\left(\frac{Df^s}{Dt}\right)_{\xi^s}$ - operator of differentiation along the trajectory of the particle free motion. I^s – model representations of the collision integral which describe birth and loss of the particles of the corresponding kind. Both elastic and nonelastic ionization electron-atom collisions are taken into account in this model. The processes of ion recombination and other types of the particle collisions are not taken into account. Integrals I^s have the same form as in [4]. A necessary requirement to any kinetic model – equations of conservation laws of mass (number of the particles and charge), impulse, energy, derived from this model, should coincide with all conservation equations that take place in this case. Above presented model complies with this requirement.

The boundary conditions for ion and neutral kinetic equations are the same as in [4]. It is assumed that ions do not enter accelerating channel and recombine on the walls. Therefore, for ion kinetic equation at all boundaries:

$$\underset{\xi_n^2>0}{f^2} = 0 \quad (3)$$

For neutrals a diffusion law of interactions with the walls with total thermal accommodation is assumed. Besides, there is a flux of neutralized ions from the walls. The particles do not penetrate the surface. There is a flux of neutrals from the anode. Then, for neutral kinetic equation:

- at the walls $f_w^3 = n_3^w \left(\frac{m_3}{2\pi k T_w}\right)^{\frac{3}{2}} \exp\left\{-\frac{m_3(\xi^3)^2}{2kT_w}\right\}$ (4a)

n_3^w - nearwall neutral density, T_w – wall temperature.

- at the anode plane $f_a^3 = f_{in}^3 + f_r^3$

$$\underset{\xi_z^3>0}{f_{in}^3} = n_3^b \left(\frac{m_3}{2\pi k T_a}\right)^{\frac{3}{2}} \exp\left\{-\frac{m_3(\xi^3-u^b)^2}{2kT_a}\right\} \quad (4b)$$

$$f_r^3 = n_3^a \left(\frac{m_3}{2\pi k T_a}\right)^{\frac{3}{2}} \exp\left\{-\frac{m_3(\xi^3)^2}{2kT_a}\right\}$$

where $n_3^b = J_b^3 / u^b$, u^b - neutral flux velocity, T_a – anode temperature. f_{in}^3 is assumed to be constant on this boundary.

- at the channel exit $\underset{\xi_z^3<0}{f^3} = 0$ (4c)

Magnetic field is one of the main factors defining the processes in SPT. Assessments show that magnetic field from the currents inside the accelerating channel

is ~10% of that one from magnetic system. Therefore this induced magnetic field is neglected and magnetic field in the model is considered as an external parameter, predefined and stationary. To obtain its value and topology in the existent SPT models a special technique was developed at RIAME MAI. Details of this technique were described in a paper [4].

That technique is based on the solving of Laplas's equation for magnetic potential $\Phi^{(m)}$, which has in cylindrical coordinate system the following form:

$$\frac{1}{r}\frac{\partial}{\partial r}\left(r\frac{\partial \Phi^{(m)}}{\partial r}\right)+\frac{1}{r^2}\frac{\partial^2 \Phi^{(m)}}{\partial \varphi^2}+\frac{\partial^2 \Phi^{(m)}}{\partial z^2}=0 \quad (5)$$

with the Neumann's boundary conditions. Normal components of the magnetic field induction are measured along the sides of the region under investigation, in the case of SPTs – along the accelerating channel walls and in the anode and cathode planes. Magnetic field is defined according to expression:

$$H = -\operatorname{grad} \Phi^{(m)} \quad (6)$$

1.2 Problem of the electric field determination

One of the main difficulties is to properly define electric field. As the magnetic field is stationary, $\operatorname{rot} E = 0$. Then

$$E = -\nabla\Phi, \quad (7)$$

Φ - electric field potential.

Expression for electric potential determination in this model is defined from the equation of impulse conservation law for electrons with the use of the idea of „thermalized potential", suggested by Morozov et al [5]. Several assumptions are made:

1) nonequilibrium adds to the stress tensor p_{ik}^1 are equal to zero;
2) electron temperature is constant along a magnetic field line.

Also, the mass conservation law for electrons is used and a unity vector $h = \frac{H}{|H|}$ is introduced. As a result a following equation was used for electric potential determination:

$$\frac{\partial \Phi}{\partial h_k} = \frac{k}{e}\frac{T_1}{n_1}\frac{\partial n_1}{\partial h_k} - 2\frac{h_k}{e}\left(\nabla_1\mu\left(u_k^3-u_k^1\right)+\nabla_1\chi(\tilde{T})m_1\left(2\tilde{u}_k-2u_k^1\right)\right) \quad (8)$$

Here k=1,2,3, ∇_1, ∇_1 - elastic and ionization electron-atom collision frequencies, correspondingly, $\mu = \frac{m_1 m_3}{m_1+m_3}$, $\tilde{u} = \frac{m_1 u^1 + m_3 u^3}{m_1+m_3}$, $\chi(\tilde{T}) = \begin{cases} 1, \tilde{T} > 0 \\ 0, \tilde{T} \le 0 \end{cases}$, $\tilde{T}$ - energetic parameter of ionization (see [4]).

For equation (8) boundary conditions were specified:
- electric field potential distribution along the internal or external cylindrical boundary;
- electron density distribution along the internal or external cylindrical boundary.

These distributions are taken from the nearwall probe measurements along the channel surface. Electric field is defined according to equation (7).

1.3 Electron dynamics

Since electron equation (impulse conservation law) was used for derivation of electric field potential equation (9), electron distribution function is not calculated in this model. But, it is necessary to have information on some electron macrocharacteristics.

Electron density is calculated from the condition of quasineutrality:

$$n_1 \approx n_2 \quad (9)$$

Electron temperature is assumed to be constant along the magnetic field line (this condition has been already used for derivation of equation (8)). Then, taking into account magnetic field topology in modern SPTs, to obtain distribution of electron temperature it is enough to specify it either on the internal wall or on the external wall of the channel.

Next, it is necessary to know distribution of electron velocity for calculation of collision integrals in (2). Assuming Maxwellian electron distribution function and characteristic electron temperature T_1^0 ~10eV, the most probable velocity, corresponding to this temperature, is $\xi_0^1 = \sqrt{\frac{2kT_1^0}{m_1}} \approx 1.9\cdot 10^6$ m/s. Electron macroscopic velocity along z-axis can be estimated from the discharge current value I_d=4.5A and near-anode electron number density $n_1 \approx 0.1\cdot 10^{18}$ 1/m^3 (typical conditions for SPT-100) as ~10^5 m/s. Drift

electron velocity – velocity in the azimuth direction – is defined as $u_\varphi^{(1)} = \frac{E}{B}$. Assuming E~$3\cdot10^4$ V/m and B~0.02Tl one can obtain $u_\varphi^{(1)} \approx 1.5\cdot10^6$ m/s. Then, taking into account all estimations, electron velocity is approximated as

$$\xi^{(1)} = \sqrt{\frac{2kT_1}{m_1}} + \frac{E_z}{B_r} \qquad (10)$$

Following made estimations, electron energy is approximated by expression

$$En_1 = \frac{3}{2}kT_1 + \frac{m_1(u_\varphi^{(1)})^2}{2} \qquad (11)$$

By this way calculated values of electron energy were used in the dependencies of the cross-sections of ionization and elastic electron-atom collisions on electron energy.

2. Results of simulation

2.1 Simulated SPT model

For the simulation an SPT-100 type model with the thrust vector control unit (TVCU) was chosen. It deviates thrust vector through the creation of azimuth nonsymmetrical magnetic field. Therefore, this model gives an excellent base to compare 3-D calculations with measurements. TVCU development objectives, its design along with the results of thrust vector deviation were presented in detail in a paper [6]. Here, in Fig.2 and 3, we present two views of that model giving its overall appearance.

SPT-100 with TVCU has one internal, four external magnetization coils (standard for SPT-100) and eight TVCU coils. Through feeding TVCU coils with the opposite directed currents a nonsymmetrical magnetic field is created.

2.2 Investigation of the magnetic field

Investigation of the magnetic field in SPT-100 with TVCU was carried out according to the technique mentioned above and presented more detailed in [4].

There were studied 3 modes of magnetization coils operation; they are listed in Table 1. Thrust vector was deviated in the horizontal plane. Boundary values of magnetic induction were measured in 7 axial cross-sections.

Table 1. Currents in magnetization coils in SPT-100 with TVCU.

No.	I_{int}, A	I_{ext}, A	I_1, A	I_2, A
1	4.2	2.1	0	0
2	4.0	2.2	+3.0	-3.0
3	3.5	2.1	+6.0	-6.0

Magnetic field topology in the plane of the thrust vector deviation for modes 2 and 3 is presented in Fig.4 and 5. One can clearly see an azimuth nonsymmetry of the magnetic field. Moreover, this nonsymmetry exists not only outside the channel but also inside it. As it was expected, the field is deformed most significantly in the mode 3; to this mode corresponds the highest angle of the thrust vector deviation.

2.3 Simulation of neutral and ion dynamics

The numerical methods for solving equation system (2,7,8) were described in detail in [4].

Values of the cross-sections of ionization and elastic electron-atom collisions for Xenon were taken from [7]. Results of the near-wall probe measurements in SPT-100 were recently reported in [8], where there were obtained distributions of electron density, temperature and electric potential along the channel external wall in the single azimuth cross-section. Under condition of the azimuth symmetrical magnetic field it is possible to assume that these distributions are reproduced at each azimuth cross-section, so there is an information on the whole surface of the external wall. Then, according to above-mentioned assumptions on „thermalized potential“, there were calculated distributions on the internal wall. Under azimuth nonsymmetrical magnetic field in the case of simulated SPT-100 with TVCU this asymmetry is minimal at the internal wall. Therefore, for calculation purposes distributions of electron temperature, density and electric potential were specified on the internal wall of the channel and assumed to have azimuth symmetry on it.

The sequence of the solution of the equations is the following.

1) Initial distributions of all macroparameters and electric field are set.
2) Ion equation from (2) is solved.
3) Then neutral equation from (2) is solved.
4) Then equation (8) for the electric field potential is solved.
Steps 2-4 are repeated on each iteration.

The program on Fortran 77 was written to realize above algorithm. In most calculations a mesh in the physical space had the following dimensions - $N_r \times N_\varphi \times N_z = 10 \times 8 \times 10$, calculation mesh in velocity space - $N_{\xi r} \times N_{\xi \varphi} \times N_{\xi z} = 34 \times 14 \times 33$ for ions and $N_{\xi r} \times N_{\xi \varphi} \times N_{\xi z} = 26 \times 20 \times 30$ for neutrals (numbering begins from zero). So, cell's dimensions for calculation in SPT-100 on r and z coordinate are 1.5mm×2mm, accordingly, and in angular coordinate - 45°. Size of the mesh was chosen to reach compromise between the accuracy and duration of calculation.

Typical distribution of electron temperature inside the accelerating channel is presented in Fig.6. One can see how the lines of equal electron temperature follow the magnetic field lines.

First, it is interesting to discuss a convergence of numerical solution procedure. Typically, there were made 22 iterations. Convergence of the whole iteration process reveals oscillations. There are oscillations of macroparameters from iteration to iteration. But the shape of distributions is reproduced. The maximal difference in charged particle density, for example, can reach ~35% and this difference is observed only in some calculation mesh nodes. Basically, the oscillations have much lower amplitude. Such a behavior of the convergence process can be explained by the following reasons.

The model does not take into account the processes of the volume recombination. For example, characteristic cross-section of the radiative recombination is $\sigma \sim 10^{-21}$ cm^2 [7], that is much lower than Xenon ionization cross-section by electron impact and elastic electron-atom collision cross-section. Volume recombination is insignificant in the region with strong electric field, at the exit from the channel, because ions leave this region rapidly. But in the near-anode region electric field is essentially weak (it is confirmed both by experiment [9] and made here calculations, see results below); in the calculation such potential distributions can appear that have the shape of a "potential trap" for ions. It leads to the situation when, some ions with low velocities do not reach the boundary of the calculation region, but "spend" long time in the volume. As a result – very high charged particle density can appear. From the physical consideration it is clear that no matter how low recombination cross-section, sooner or later ion will recombine if it sufficiently long "travels" in the volume of the plasma.

The next reason that can define the above described convergence character – obtained expression (8) for potential has a disadvantage. From that expression follows that electric field magnitude, and correspondingly distributions of ion macroparameters, does not depend on magnetic field magnitude but only on its topology. It seems to be dubious because electric field in plasma is defined by the charged particles distribution and electron component's parameters depend significantly on magnetic field magnitude. Moreover, magnetic field in the near-anode region has one order of magnitude less than in the ionization and acceleration region. Electron Larmour radius turns out to be large comparatively to the width of the channel and the "thermalized potential" approach in this region can result in the great errors.

Nevertheless, the main criteria, which allow us to estimate the validity of the calculation results – thrust and thrust vector direction – are in satisfactory agreement with the experiment. For the mode 2 (see Table 1) calculated mean value of the thrust is 66.3mN with measured in the experiment value 72.1mN. For the mode 6 the mean value is 46.5mN with measured in experiment value 68.1мН. In average, calculated thrust value is lower than measured one; it can be explained by the following reasons. Firstly, in the presented model there are no doubly-charged ions. Their share in the SPT-100 plume, for example, can reach 11%, according to [10]. Secondly, ionization mechanisms other than ionization by electron impact from the ground level are not taken into account, in particular ionization through excitation levels. Thirdly, as it can be seen from Fig.17 and 18 acceleration region on some radii continues out of the calculation region and these parts were not taken into account. From the presented results one can clearly see that calculated thrust for the mode 3 differs more significantly from the measured one than for the mode 2. This can be related to the fact that magnetic field topology for this mode has stronger azimuth nonuniformity, accordingly the use of the experimental data on the near-wall electron temperature distribution obtained under azimuth-symmetrical magnetic field, gives greater error. Thrust vector deviation angle mean value is 2.3° in the first case with measured in experiment 2.6°, in the second case it is 5.2° with measured in experiment 4.8°.

Ion current mean value is 2.96A for the mode 2, for the mode 3 it is 2.28A. As electron component under this problem statement is not calculated, and therefore it is difficult to estimate discharge current.

Further in Fig.7-18 there are represented calculated distributions of macroparameters in the accelerating channel in the horizontal plane, corresponding to the plane of thrust vector deviation, for the mode 3 because for it the azimuth asymmetry is more pronounced. Horizontal axis z is in the direction of the accelerating channel walls, vertical – r, all macroparameters are in dimensionless form. z=0 corresponds to the plane placed 4mm from the anode into the channel, z=1 - to the channel cut-off plane (L=20mm).

Discussion

It is necessary to point out that there is limited number of reliable experimental data on macroparameters distribution in the SPT discharge chamber. This is because of the difficulty in experiment conduction and subsequent result interpretation in plasma placed in the crossed electric and magnetic fields. Therefore it is possible to compare only in approximate way the obtained calculated results with measured macroparameters distribution in various SPT models. Among known works it is worth to mention investigations by Bishaev A.M., Kim V. [9] and recently presented results by J.M.Haas, A.L.Gallimore [11].

Calculated charged particles density distributions (Fig.7-8) are qualitatively consistent with the distributions obtained in [9,11] by probe diagnostics. The maximal density is observed near the exit of the channel and placed mostly in the region of the positive magnetic field gradient. The order of magnitudes is also in good agreement $\sim 10^{18}$ $1/m^3$. Interesting to note, that if one takes a density distribution as a dependence on longitudinal coordinate z at any fixed radius, for instance r=1.98 (see Fig.8), then one clearly sees two local maximums. Such a character of the distributions is observed in experiments [11]. In the upper part of cross-section in Fig.5 at the external wall magnetic field lines are tilted inside the channel, then in the Fig.7 one can note the displacement of the zone with charged particles maximal density toward the anode. Density magnitude in this cross-section is less than in the opposite cross-section (Fig.8).

Analyzing the character of the calculated ion flux distribution it is possible to point out the existence of the reverse ion fluxes (toward the anode) (Fig.9-10). Such fluxes were experimentally obtained in [9]. Also, the calculation gives considerable ion fluxes toward the accelerating channel walls (Fig.12-13), especially on the internal wall. High values of the ion fluxes toward an internal wall were registered in experiment [9]. Radial flux magnitude can reach ~20% of that one in longitudinal direction at the exit of the channel and in the ionization region these fluxes can have a comparable magnitude. It seems to be reasonable that radial ion fluxes have the greatest value in the ionization region because here considerable density gradients are observed, and correspondingly, strong radial electric fields. In Fig.11 there is represented the ion flux z-component distribution on azimuth at the exit cross-section. The highest values are observable at the azimuth angle 270°, i.e. in the cross-section with magnetic field lines deformed to the exit of the channel (lower part of Fig.5). In this cross-section there are the highest ion fluxes toward the channel walls, especially toward the internal one (see Fig.13). This fact is in a well agreement with the result of highest charged particle density. Directed ion flux structure is presented in Fig.14, the scale in the left and right part of the figure is different.

Calculated neutral density (see Fig.15-16) has local maximums near the walls. It follows from the accepted ion-wall interaction model, according to which ions reflect as neutrals. Density local maximums are observed correspondingly in the region of the highest ion fluxes. Qualitatively such a picture was obtained in the investigation [12].

Electric field potential distribution (see Fig.17-18) repeats the shape of the near-wall potential distribution, which is used as boundary condition for equation (8), and magnetic field topology (comp. with Fig.5). Such a sharp drop of the potential was observed in experiment – see [11]. In the most part of the channel the variation of the potential is weak, correspondingly the electric field is also weak.

Ion distribution function on the longitudinal velocity component ξ_z (see Fig.19) in the internal point of the channel has the maximum near zero – it is a consequence of the weak electric field in this region. Corresponding directed ion velocity u_z=-0.0057, i.e. ion flux is directed toward the anode. Ion temperature is T_2=0.005 or 1.5eV. At the exit cross-section corresponding directed velocity u_z=0.68, temperature - T_2=0.035 or 10.5eV. Calculated ion temperature at exit cross-section is on the order of electron temperature.

Conclusions

Presented 3-dimensional model of atom and ion dynamics in SPT accelerating channel is based on the

model kinetic equations. It takes directly into account only a limited number of the physical processes in the SPT plasma volume – electron impact ionization, elastic electron-atom collisions. Nevertheless, there were obtained a satisfactory quantitative agreement with the experimental results: on thrust, thrust vector deviation angle for two different SPT operation modes. Calculated macroparameters distributions are in a qualitative agreement with experimentally obtained ones for different SPTs. In particular, reverse ion fluxes toward the anode and considerable ion fluxes toward the accelerating channel walls were obtained.

The expression for the electric field determination in this model was obtained from the equation of electron impulse conservation law with the use of "thermalized potential" assumption. Therefore electron dynamics was specified on the base of available experimental data. The strongest electric field was obtained in the region with high magnitudes of electron temperature and magnetic field, i.e. near the exit of the channel. In the near-anode region magnetic field has the order of magnitude less than in the rest of the channel, therefore obtained expression with "thermalized potential" can lead to a large error in electric field calculation; but the field is small in this region.

There are oscillations during the iteration process; the possible reason of this is the absence of a volume recombination mechanism in the model.

To describe ionization and acceleration process in SPT more accurately it is necessary to expand the calculation region out of the channel. Ionization and acceleration mechanisms have an essentially non-stationary character, therefore solution of the non-stationary problem will be the future step of investigations.

Acknowledgments

This work was supported by German Service of Academic Exchanges (DAAD).

References

[1] K.Komurasaki, Y.Arakawa "two-Dimensional Numerical Model of Plasma Flow in a Hall Thruster" – *Journal of Propulsion and Power, Vol.11, 1995, pp.1317-1323.*

[2] P.Boeuf and L.Garrigues „Low frequency oscillations in a stationary plasma thruster" – *Journal of Applied Physics, 1998, vol. 84, Nr. 7, pp. 3541-3554.*

[3] I.D.Boyd, L.Carrigues, J.Koo, M.Keidar „Progress in Development of a Combined Device/Plume Model for Hall Thrusters" – *AIAA-2000-3520, USA, Huntsville, July 2000.*

[4] A.M.Bishaev, V.Kim, A.V.Lazourenko „Simulation of Plasma Dynamics in SPT" – *Proceedings of 3rd International Conference "Space Propulsion", Cannes, France, 2000.*

[5] A.I.Morozov, Yu.V.Esipchuk, G.N.Tilinin et al. „Experimental investigation of the accelerator with closed electron drift and prolonged acceleration zone" (in Russian) – *ZhTF, 1972, XLII, №1, pp.54-63.*

[6] M.Day, V.Kim, V.Kozlov, A.Lazourenko et al "Investigation of the possibility to reduce SPT plume divergence by optimization of the magnetic field topology in the accelerating channel" – *IEPC-97-154, Cleveland, Ohio.*

[7] M.Mitchner, Ch.H.Kruger,Jr. „Partially Ionized Gases" – *John Wiley & Sons, Inc., 1973.*

[8] V.Kim, V.I.Kozlov, A.V.Lazourenko, A.I.Skrylnikov, N.Gascon „Investigation of Local Plasma Parameter Distributions along the SPT Accelerating Channel under Different External Electric Circuit Parameters" – *in the proceedings of 3rd International Conference "Space Propulsion", Cannes, France, 2000.*

[9] A.M.Bishaev, V.Kim „Investigation of the plasma local parameters in the accelerator with closed electron drift and prolonged acceleration zone" (in Russian) – *ZhTF, 1978, 48, №9, pp. 1853-1857.*

[10] L.B.King, A.D.Gallimore „Mass Spectral Measurements in the Plume of an SPT-100 Hall Thruster", *AIAA Journal of Propulsion and Power, 2000, Nov.-Dec., vol. 16, No. 6, pp. 1086-1092.*

[11] J.M.Haas, A.D.Gallimore "An Investigation of Ion Number Density and Electron Temperature Profiles in a Laboratory-Model Hall Thruster" – *AIAA 00-3422 USA, Huntsville, July 2000.*

[12] A.M.Bishaev, V.Kim „Investigation of the influence of the wall configuration on plasma parameters distribution in UZDP" (in Russian) – *in the book: Plasma sources and accelerators, Kharkov: KhAI,1981, v.5, pp. 3-8.*

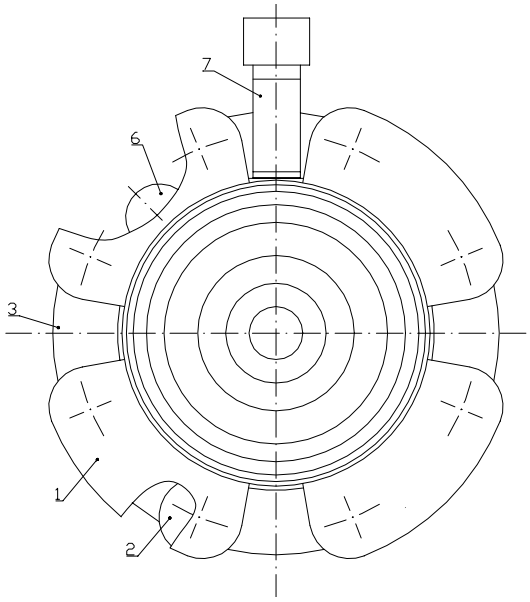

Fig.2 Rear view of the simulated SPT-100 model with TVCU.
1 – additional external magnetic poles of TVCU; 2 – additional magnetization coils; 3 – main external pole; 6 – main external magnetization coils; 7 – cathode.

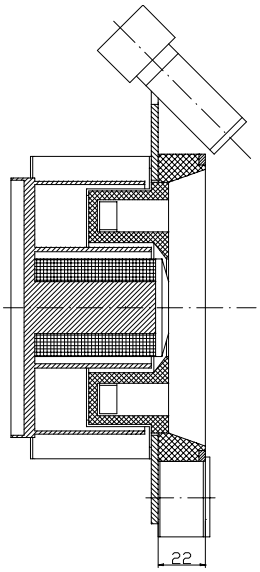

Fig.3 Cross-section of the simulated SPT-100 model with TVCU.

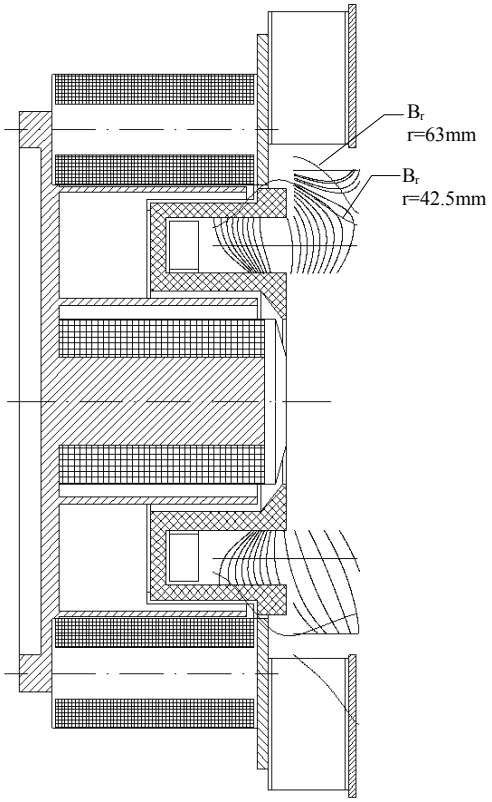

Fig.4.
Magnetic field in the axial cross-section, mode 2.

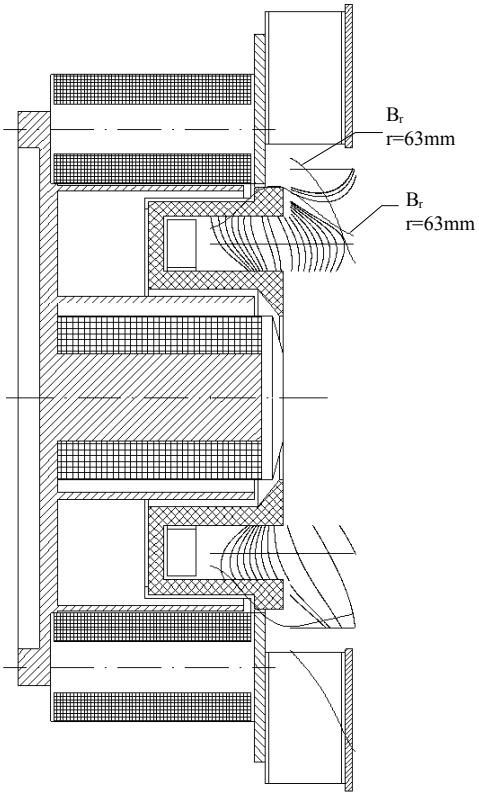

Fig.5.
Magnetic field in the axial cross-section, mode 3.

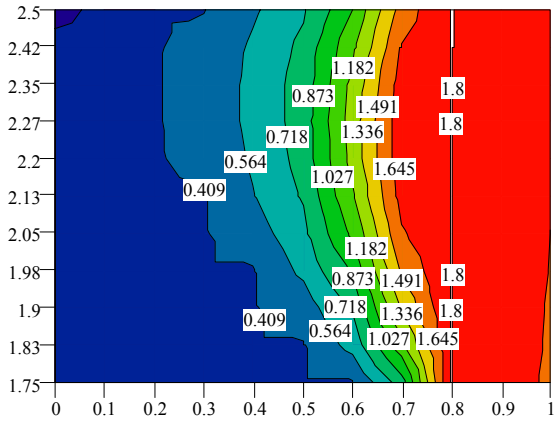

Fig.6. Example of electron temperature distribution in the accelerating channel (r-z plane, horizontal axis – z, vertical one - r). in dimensionless form, T_1^0=10eV.

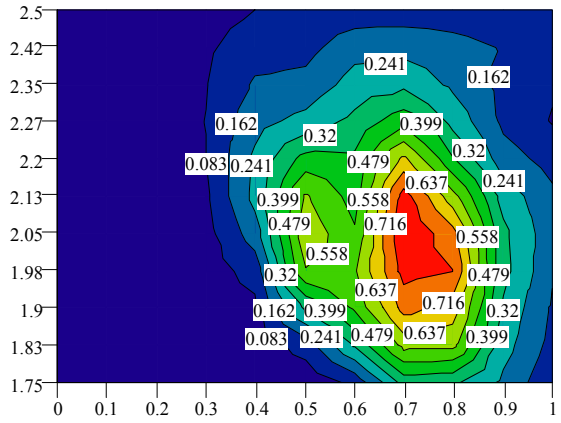

Fig.7 Charged particle density distribution, corresponds to the upper part of Fig.5; $n_1^0 = n_2^0 = 1 \cdot 10^{18}$ 1/m^3.

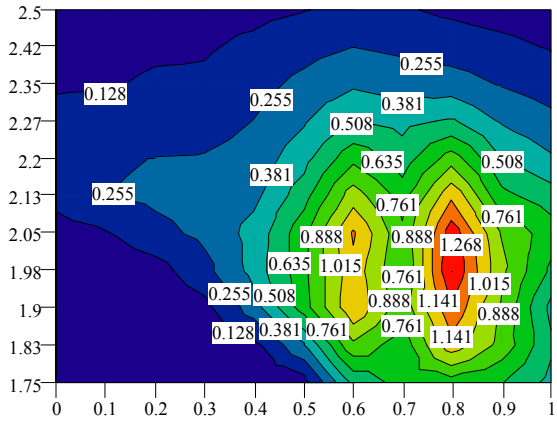

Fig.8 Charged particle density distribution, corresponds to the lower part of Fig.5; $n_1^0 = n_2^0 = 1 \cdot 10^{18}$ 1/m^3.

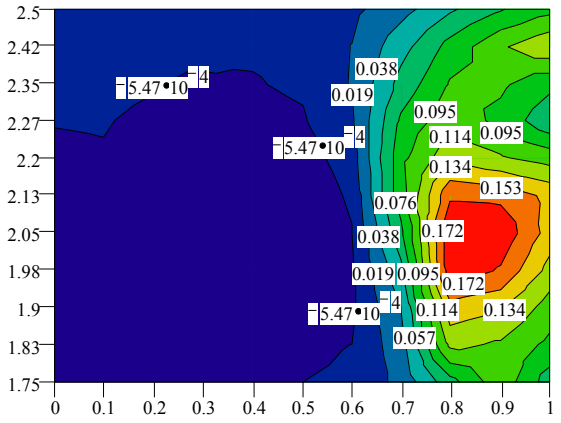

Fig.9 Ion flux density, z-component, corresponds to the upper part of Fig.5; $(nu)_2^0 = 2.1 \cdot 10^{22}$ 1/(m^2·s).

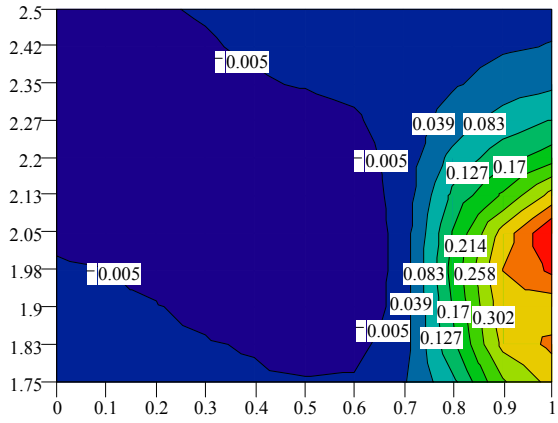

Fig.10 Ion flux density, z-component, corresponds to the lower part of Fig.5; $(nu)_2^0 = 2.1 \cdot 10^{22}$ 1/(m^2·s).

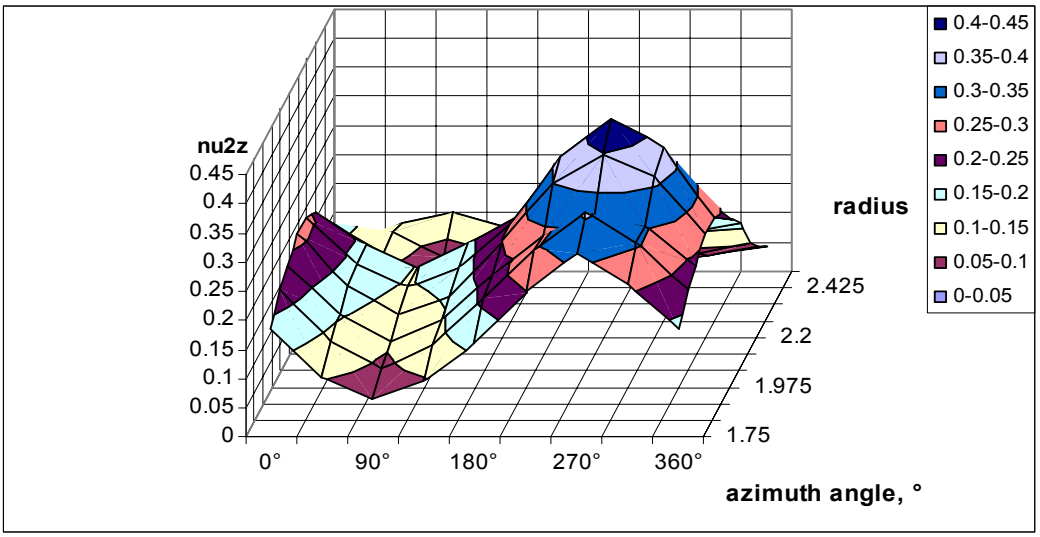

Fig.11 Ion flux density, z-component, at the exit cross-section of the channel (z=1), distribution on azimuth and radius; $(nu)_2^0 = 2.1 \cdot 10^{22}$ 1/(m^2·s).

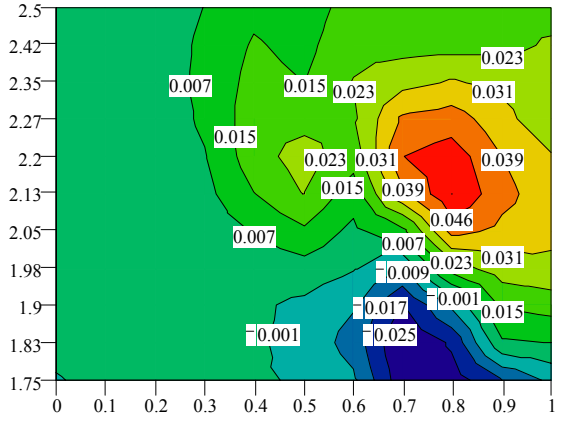

nu2r2

Fig.12 Ion flux density, r-component, corresponds to the upper part of Fig.5; $(nu)_2^0 = 2.1 \cdot 10^{22}$ 1/(m^2·s).

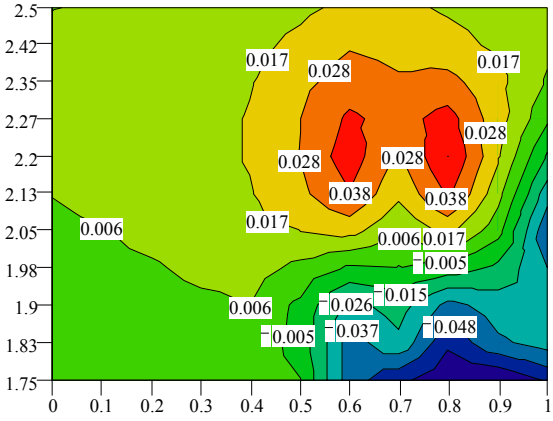

nu2r6

Fig.13 Ion flux density, r-component, corresponds to the lower part of Fig.5; $(nu)_2^0 = 2.1 \cdot 10^{22}$ 1/(m^2·s).

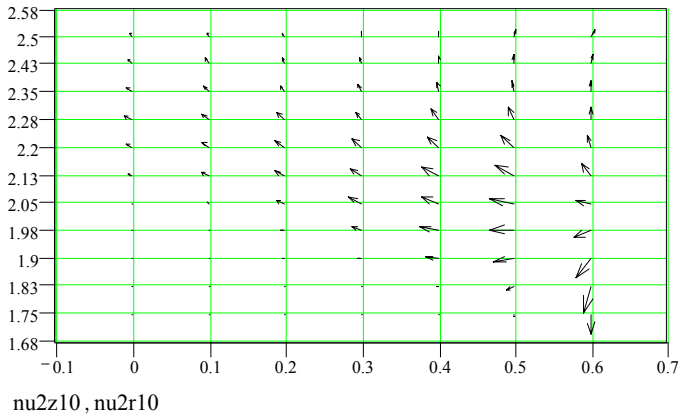

nu2z10 , nu2r10

a) near-anode region.

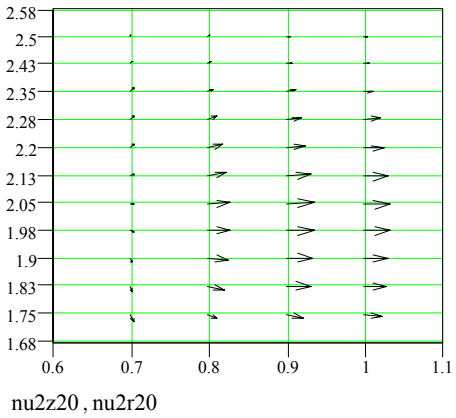

nu2z20 , nu2r20

b) exit region.

Fig.14 Ion currents structure, figures a and b – different scales.

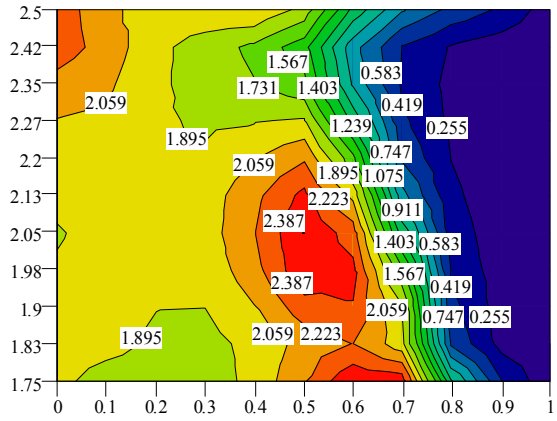

n32

Fig.15 Neutral density distribution, corresponds to the upper part of Fig.5; $n_3^0 = 1.7 \cdot 10^{19}$ 1/m^3.

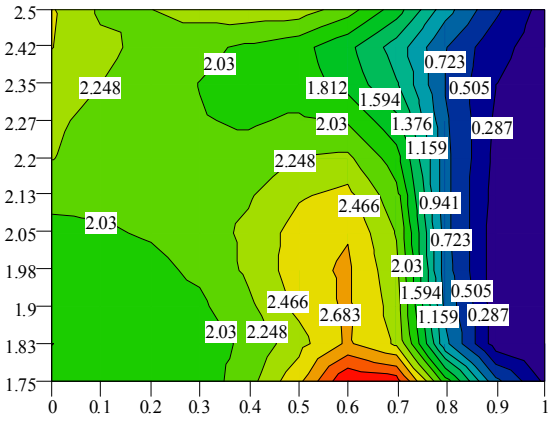

n36

Fig.16 Neutral density distribution, corresponds to the lower part of Fig.5; $n_3^0 = 1.7 \cdot 10^{19}$ 1/m^3.

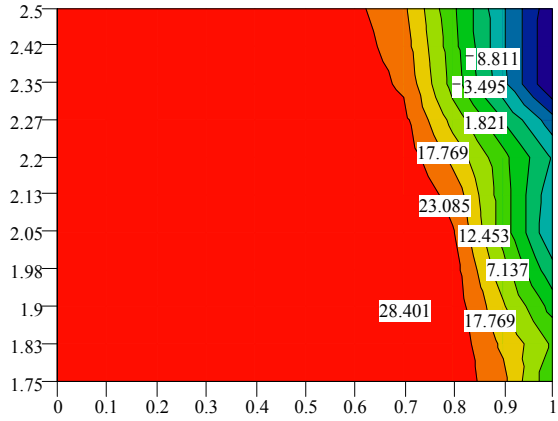

f2

Fig.17 Electric field potential distribution, corresponds to the upper part of Fig.5; Φ_0=10V.

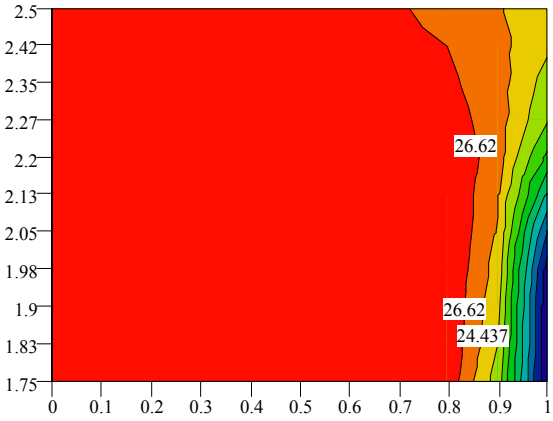

f6

Fig.18 Electric field potential distribution, corresponds to the lower part of Fig.5; Φ_0=10V.

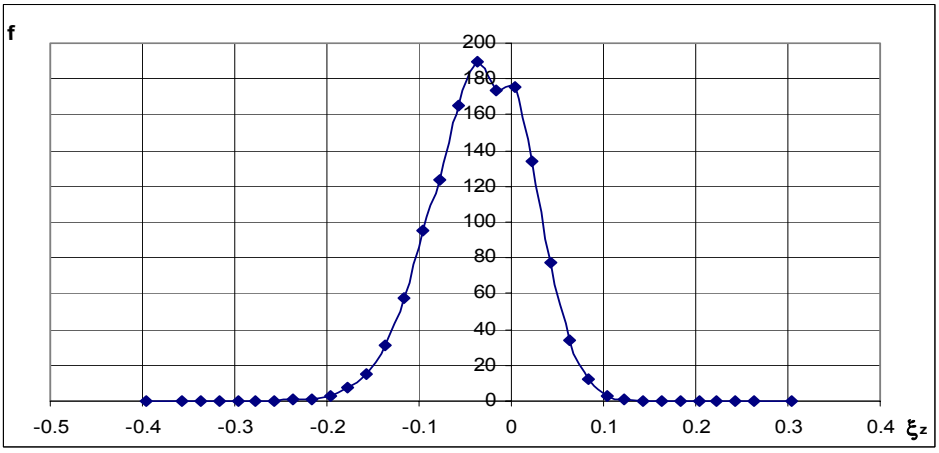

Fig.19 Ion distribution function on z-component ξ_z of the velocity, channel internal point z=0.5, r=2.125 (ξ_r=-0.0017, ξ_φ=0.0021).